

Topotaxis of active particles across long distances by sliding along obstacles

Zeinab Sadjadi^{1,*} and Heiko Rieger^{1,2}

¹*Department of Theoretical Physics & Center for Biophysics, Saarland University, 66123 Saarbrücken, Germany*

²*Leibniz Institute for New Materials INM, 66123 Saarbrücken, Germany*

 (Received 3 May 2023; revised 31 October 2023; accepted 16 January 2024; published 20 February 2024)

Many biological active agents respond to gradients of environmental cues by redirecting their motion. In addition to the well-studied prominent examples such as phototaxis and chemotaxis, there has been considerable recent interest in topotaxis, i.e., the ability to sense and follow topographic environmental cues. A trivial topotaxis is achievable through a spatial gradient of obstacle density, though over limited length scales. Here, we introduce a type of topotaxis based on sliding of particles along obstacles—as observed, e.g., in bacterial dynamics near surfaces. We numerically demonstrate how imposing a gradient in the angle of sliding along pillars breaks the spatial symmetry and biases the direction of motion, resulting in an efficient topotaxis in a uniform pillar park. By repeating blocks of pillars with a strong gradient of sliding angle, we propose an efficient method for guiding particles over arbitrary long distances. We provide an explanation for this spectacular phenomenon based on effective reflection at the borders of neighboring blocks. Our results are of technological and medical importance for design of efficient taxis devices for living agents.

DOI: [10.1103/PhysRevResearch.6.013178](https://doi.org/10.1103/PhysRevResearch.6.013178)

I. INTRODUCTION

Biological microswimmers, migrating cells, and other living organisms can sense and follow topographic cues of the environment and respond by adapting their dynamics. This feature, which is called topotaxis, has attracted considerable attention [1–8], as it does not rely on the influence of any specific stimulus on the internal self-propulsion mechanism of the agent; it is solely based on the physical interactions with and properties of the surrounding environment such as spatial arrangement of obstacles, degree of lateral confinement, and surface topography. For a more efficient navigation, these features may be exploited by biological organisms—particularly by immune cells, as they are responsible for exploring extracellular matrices and confined tissues to detect pathogens [9–14]. So far, topotaxis has been reported in the presence of a spatial gradient of either obstacle density [1–5] or substrate topography (for free motion on surfaces) [6,7]. It is unclear whether spatial variation of other topographic features can lead to an efficient taxis. Moreover, the topotaxis induced by such features is practically applicable only on short length scales: A gradient over a long distance will be so weak that the taxis device becomes inefficient for single runs. A weak net flux can be obtained only by statistically averaging over long times and large ensembles. Additionally, inducing an extremely weak gradient of any topographic feature requires high fabrication precision, which is challenging at least at microscale.

Living organisms interact with obstacles in different ways. For instance, swimming bacteria may be hydrodynamically captured by and slide along surfaces [15–17], migrating or killer cells are often temporarily trapped near obstacles [2,18–20], and microalgae push their flagella against surfaces and scatter [21–23]. While the diffusivity may be enhanced by sliding around the objects [16], it is reduced by being trapped near obstacles or scattered from them [24–29]. A detailed understanding of how the existence or strength of topotaxis depends on the interplay between topographic cues and the nature of agent-obstacle interaction is currently lacking.

Here, we study the motion of active agents in obstacle parks consisting of regularly arranged circular pillars. The density of pillars is the same throughout the system to prevent possible drifts due to obstacle density variations. We impose a gradient of topographic stimulus by varying the particle-obstacle interactions throughout the obstacle park, which is implemented through the sliding around pillars. Although this particular sort of motion is limited to a class of active objects that physically interact with obstacles, it constitutes an important class of biological agents including swimming bacteria and migrating (immune) cells. By performing extensive numerical simulations of a persistent random walk (PRW) with two distinct states in the bulk and in the vicinity of obstacles [30–32], we verify that the interplay between self-propulsion of the moving agents, agent-obstacle interactions, and topographical cues in the environment determines the possibility and strength of an effective topotaxis along the imposed gradients.

II. MODEL

We consider a two-dimensional medium consisting of circular pillars placed on a square lattice; see Fig. 1. We model the motion of the self-propelled agents by a PRW. The walkers

*sadjadi@lusi.uni-sb.de

Published by the American Physical Society under the terms of the Creative Commons Attribution 4.0 International license. Further distribution of this work must maintain attribution to the author(s) and the published article's title, journal citation, and DOI.

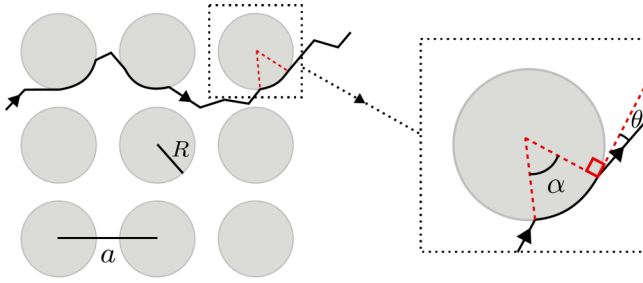


FIG. 1. Schematic drawing of a sample trajectory in a pillar array with lattice constant a and pillar radius R . The sliding and leaving angles are denoted with α and θ , respectively.

move with a constant step length l at each time step. We define the mean local persistence as $p = \langle \cos \phi \rangle$ [33], with ϕ being the turning angle between the successive steps and $\langle \dots \rangle$ denoting the average with respect to the turning-angle distribution $R(\phi)$. The persistence values $p = 1$ and 0 correspond to ballistic and purely diffusive motion, respectively. We introduce a sliding boundary condition on the pillar surfaces. After collision, the walker moves along the obstacle surface with an angle α and leaves the obstacle surface with angle θ from the tangent of the circle; see Fig. 1. Here, θ is uniformly chosen from $[0, \frac{\pi}{4}]$. We checked that the choice of θ has no influence on the observed trends and our conclusions. While the free parameter α can be pillar-size dependent in general [15], here, α is independent of R .

We perform Monte Carlo simulations of migration through the pillar park. The simulation box is $300l \times 300l$, in which the pillars are arranged on a square lattice with lattice constant $a = 12.5l$. A circular pillar with radius R is placed on each lattice point (24 pillars in each row or column). By changing R , we vary the occupied fraction by pillars (characterized by the dimensionless parameter $\lambda = 2R/a \in [0, 1]$). An event-driven algorithm is applied, where every collision with an obstacle is considered a new event. The particle takes a step with length l , unless it collides with an obstacle. In the case of no collision, the walker takes a new direction drawn from $R(\phi)$, which is chosen to be uniform over $[\phi_0, \phi_1]$. The values of the angles ϕ_0 and ϕ_1 can be tuned to get the desired persistence p . An ensemble of 10^5 random walks (RWs) with random initial position and direction are considered, and periodic boundary conditions are applied. To induce topotaxis, we consider a constant sliding angle α around each pillar but impose a gradient of α in the medium.

III. RESULTS

To understand the influence of the geometric parameters α and λ on the particle migration in pillar parks, we study the behavior of the effective diffusion constant D at a given α and vary λ by changing the radii of obstacles. Since the diffusion constant in free space D_0 depends on the persistence as $D_0 \propto \frac{1+p}{1-p}$ [34], in the following, we rescale D as $\tilde{D} = D/D_0$ to eliminate the role of p . In Figs. 2(a) and 2(b), \tilde{D} is plotted vs λ for different values of α . The results are presented for $p = 0$ and 0.5 . Typical behavior of the mean square displacement (MSD) in the steady state (from which D

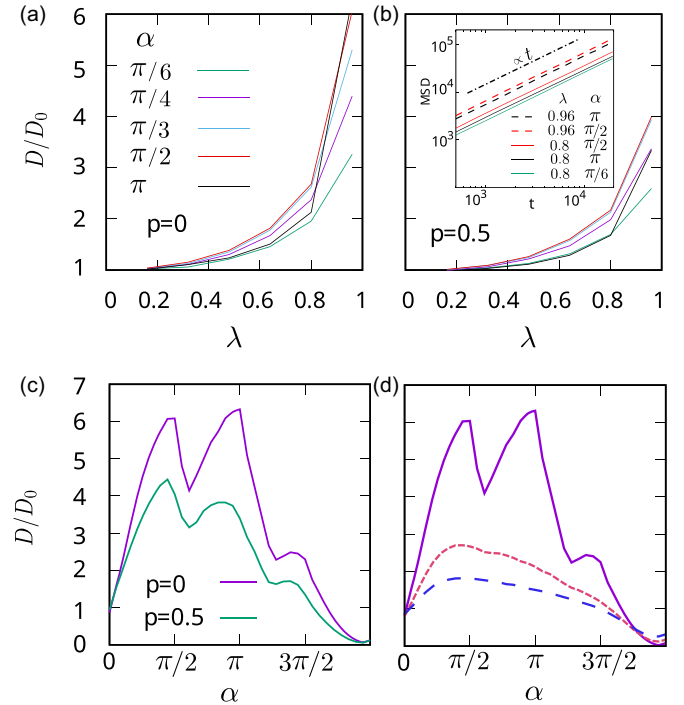


FIG. 2. Rescaled diffusion constant vs $\lambda = 2R/a$ for (a) a normal random walk (RW) and (b) a persistent RW (PRW) with persistence $p = 0.5$. Each color represents a fixed sliding angle on the obstacle surface. Inset: Typical MSD(t) for $p = 0.5$. (c) D/D_0 vs α for a normal and persistent RW. (d) D/D_0 vs α for normal RW in pillar parks with various pillar densities. The full, dotted, and dashed lines represent $\lambda = 0.96, 0.8$, and 0.64 , respectively.

is extracted) is shown in the inset of Fig. 2(b). We observe that D grows with λ , and its variation is affected by the choice of α . Without sliding along obstacle surfaces, e.g., with reflective boundary conditions on pillar surfaces, \tilde{D} decreases with pillar density, which is a known result [29]; however, when sliding along the obstacle surface is allowed, \tilde{D} interestingly increases with density. For dense packing, the displacement $R\alpha$ on the perimeter of a pillar is larger than the pillar spacing. Moreover, in denser pillar parks, where random walkers are trapped between pillars, they use the sliding on the pillar surface to escape the traps and propagate faster between pillars. In the case of PRW [Fig. 2(b)], with the same α as for $p = 0$, we observe a weaker increase in the relative diffusion constant. This is because active agents are less frequently trapped between pillars due to their active motion; thus, the relative impact of sliding on diffusion coefficient is less pronounced. In Fig. 2(c), \tilde{D} of normal and persistent RWs is plotted vs α in a dense pillar park with $\lambda = 0.96$. We observe three peaks at multiples of $\frac{\pi}{2}$. The maximum value of \tilde{D} is located either at $\alpha = \frac{\pi}{2}$ or $\alpha = \pi$, depending on the persistence of the random walker. However, this behavior disappears in smaller packing fractions, as shown for $p = 0$ in Fig. 2(d). A similar trend is observed for $p > 0$. Thus, for sufficiently large λ , the impact of geometrical properties of the pillars (e.g., α) on the diffusion constant are more pronounced. Based on these findings, we hypothesize that a gradient of the sliding angle through dense pillar parks can lead to topotaxis.

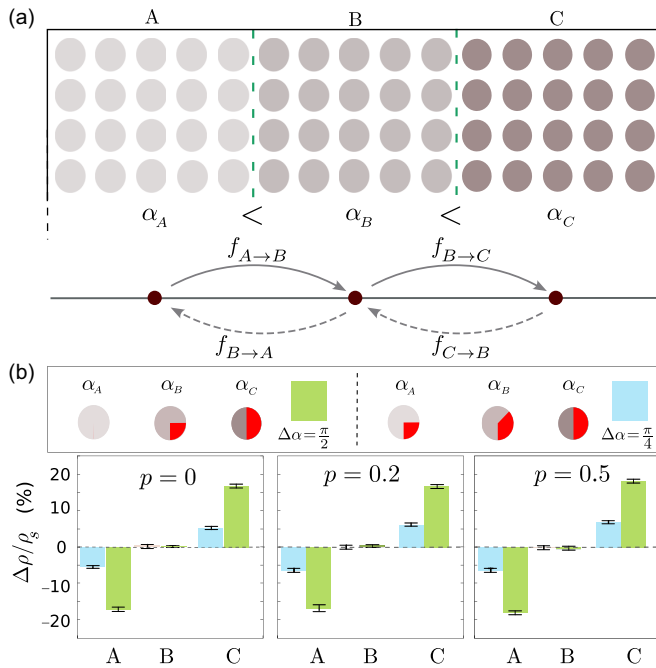


FIG. 3. Inducing taxis in an obstacle park with homogeneous packing fraction by varying the sliding angle. (a) Schematic representation of an obstacle park with piecewise changing of sliding angle α . A different value of α is assigned to each zone, with zone A (C) having the smallest (largest) angle. The color intensity of pillars is proportional to α . The lower panel depicts a one-dimensional (1D) asymmetric random walk (RW) model with unequal transition probabilities for hopping to right and left. (b) Relative particle density in each zone (with respect to the homogeneous stationary density ρ_s) for normal and persistent RWs for two sets of α_A , α_B , and α_C shown by green and blue, at $\lambda = 0.96$.

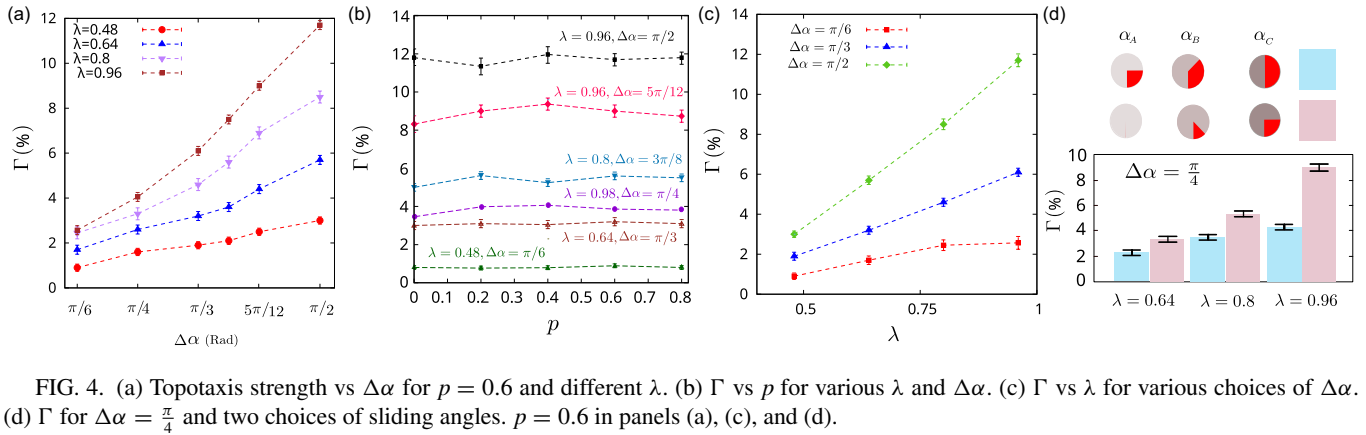
To induce topotaxis in a homogeneous medium with uniform packing fraction, we consider a monodisperse pillar park and assume that the sliding angle of the particles along the pillars can be tuned by adapting the surface properties, e.g., by means of different coatings. We divide the medium into parallel sections and assign a constant α to each section. Here, we present the results for choosing three zones A, B, and C with $\alpha_A < \alpha_B < \alpha_C$, as depicted in Fig. 3(a). Note that, due to periodic boundary conditions, sections A and C are also neighbors. We define particle density ρ as the number of random walkers per unit of available area (i.e., pillar area excluded). We let the particles migrate in the medium, starting from random positions and orientations. In a homogeneous medium, one expects to have $\rho_A = \rho_B = \rho_C \equiv \rho_s$, with $\rho_s = \frac{1}{3}$ being the particle density in the steady state of a homogeneous pillar park. Here, we observe $\rho_A < \rho_B < \rho_C$, which means that the particles preferentially reside in the zones with larger α . Interestingly, this tendency mainly depends on the values of sliding angles (in a given λ) rather than the persistence of the random walker. A larger difference $\Delta\alpha$ between the sliding angles in adjacent zones results in a larger difference in the steady particle densities ρ_A , ρ_B , and ρ_C . In Fig. 3(b), exemplary variations of the relative density $\Delta\rho = \rho - \rho_s$ are shown in different zones in the steady state. The results are presented for $p = 0$, 0.2, and 0.5 and two

choices of sliding angles, as depicted by red in the figure. For simplicity, we assume that the differences between sliding angles in the two neighboring zones are the same, i.e., $\Delta\alpha = |\alpha_A - \alpha_B| = |\alpha_B - \alpha_C| = \frac{1}{2}|\alpha_A - \alpha_C|$. In examples shown in Fig. 3(b) with green and blue colors, $\Delta\alpha$ equals $\frac{\pi}{2}$ and $\frac{\pi}{4}$, respectively. For all choices of persistence, a positive (negative) $\Delta\rho$ in section C (A) in the steady state shows that more (less) particles are found there. Moreover, a larger $\Delta\alpha$ (green) results in a significantly larger $|\Delta\rho/\rho_s|$ than the one with a smaller $\Delta\alpha$ (blue). This result indicates a taxis from smaller to larger α emerges with a strength which depends on $\Delta\alpha$. This can be mapped into a one-dimensional (1D) asymmetric RW model where each slot is represented by a site with asymmetric transition probabilities to the neighboring sites [see Fig. 3(a)]. We checked that other (inhomogeneous) initial conditions lead to similar conclusions. The result illustrated by Fig. 3(b) is somewhat counterintuitive since sliding with larger angles is reminiscent of active particles attaining higher activity or self-propulsion—which leads in active Brownian particle systems to a depletion of particles [35], contrary to what happens here—and we will clarify the reason below.

To better understand how the topotaxis strength depends on $\Delta\alpha$ and λ , we quantify the strength of taxis Γ by the maximum difference between the steady densities, i.e., $\Gamma = \rho_C - \rho_A$. In Fig. 4(a), Γ is plotted vs $\Delta\alpha$ for different values of λ for a given p . We set $\alpha_C = \pi$ and vary $\Delta\alpha$ (i.e., choose $\alpha_A = \pi - 2\Delta\alpha$ and $\alpha_B = \pi - \Delta\alpha$). Here, Γ shows a nearly linear dependence on $\Delta\alpha$ which is stronger for larger λ . Even for middle values of λ , a significant topotaxis can be achieved by choosing proper parameters. Figure 4(b) shows Γ vs p for various choices of λ and $\Delta\alpha$. It can be clearly seen that Γ is independent of persistence, while it strongly depends on the choice of the geometrical parameters λ and $\Delta\alpha$. Here, Γ is also plotted vs λ in Fig. 4(c), which shows that increasing λ enhances the topotaxis strength, and the effect is more pronounced for larger $\Delta\alpha$.

We note that, for a given choice of $\Delta\alpha$, there is a degree of freedom to choose the set of the sliding angles of the zones. An example for $\Delta\alpha = \frac{\pi}{4}$ and two choices of sliding angles is shown in Fig. 4(d). Interestingly, Γ depends not only on $\Delta\alpha$ but also on the chosen range of the sliding angles. Denoting the minimum sliding angle by $\alpha_{\min} \equiv \alpha_A$, we observe that choosing a smaller α_{\min} leads to a larger Γ . Thus, for given values of $\Delta\alpha$ and λ , the maximum topotaxis strength is achieved for $\alpha_{\min} = 0$, i.e., no sliding on the pillars.

In an inhomogeneous environment, particles tend to gather in regions where they have a lower mobility, i.e., smaller D [36]. Therefore, the trivial way to induce topotaxis is to apply a gradient of the packing fraction of obstacles, which changes the local available space for migration. This way, the density of particles will be higher in regions with larger obstacle density, where particles have smaller D due to frequent reflections. However, our findings demonstrate a counterintuitive possibility. We induce accumulation in zones with larger sliding angles, which have a larger D [see Fig. 2(c)]. To provide a qualitative understanding of the underlying mechanism, we focus on the interface between two zones with different sliding angles $\alpha_1 < \alpha_2$. In Fig. 5(a), a sample trajectory in the extreme case of $\alpha_1 = 0$ and $\alpha_2 = \pi$ is depicted. Starting



in region 1 (i.e., left), the particle is often trapped between the obstacles due to frequent reflections from them. However, when it enters region 2 with the possibility of sliding on pillars, it can be effectively pulled into the medium by sliding around many pillars without being locally trapped. If one waits enough, the particle returns to the interface again, as shown in Fig. 5(b) for different choices of p , α_1 , and α_2 . While these sample random walkers have the chance to reenter region 1, the interface acts as a pseudoreflective wall and effectively guides them back to region 2.

Toward practical applications, such as guiding biological agents inside channels, particles should be guided in a specified direction over long distances. To this aim, one could partition the system into many blocks with successively increasing α . However, this corresponds to small $\Delta\alpha$ between

neighboring blocks, thus, a weak effective topotaxis [see Fig. 4(a)]; indeed, $\Gamma \rightarrow 0$ for $\Delta\alpha \rightarrow 0$. We exploit this feature by partitioning a long strip into several blocks and let α decrease from π to 0 in each block, as shown in Fig. 5(c), and apply periodic boundary conditions. Consequently, while the particles experience a topotaxis within each block, they are pulled into the neighboring block at the interface with $\Delta\alpha = \pi$. The transition rates from all interfaces (including the one with periodic boundaries) are similar; thus, all transitions between the blocks have a bias to the right and create a circular flux. In contrast, in the setup of Fig. 3(a), the transition across the periodic boundary is in the opposite direction at other interfaces, leading to an accumulation of particles in the right-most stripe. We measure the net flux by counting the number of particles passing cross-sections at different positions per

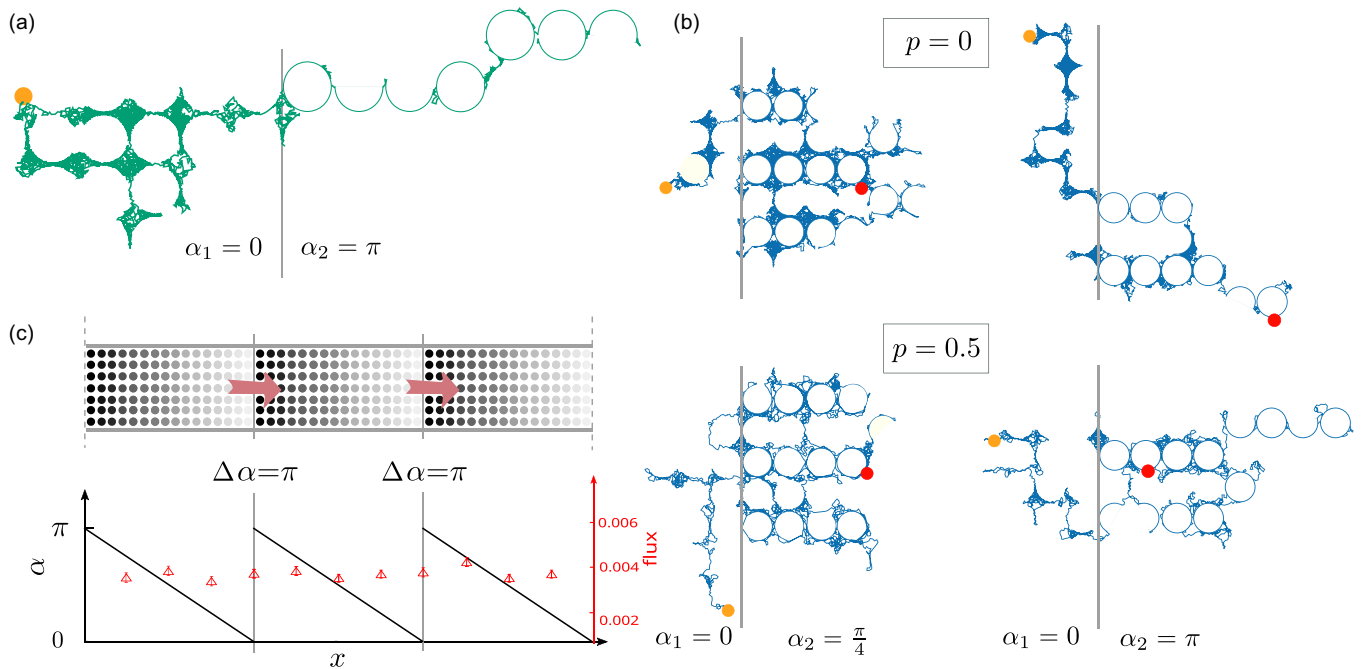


FIG. 5. (a) An exemplary trajectory at the interface of two zones with different α . The orange circle depicts the starting point. (b) Examples of longer trajectories where the random walker has enough time for several returns to the interface. Different panels represent either normal or persistent random walks (RWs) for two choices of sliding angles α_1 and α_2 . The orange and red circles represent the starting and final position, respectively. (c) Schematic design for guiding particles through blocks of pillars with a linear decrease of α in each block, represented with decreasing color intensity. Arrows show the direction of the net flux. The net flux (per length unit) is shown at different cross-sections (red triangles).

time step along the channel. We obtain a significant flux of particles in the steady state, from left to right; for instance, the result is shown in Fig. 5(c) for initial density of ~ 1 particle per unit area. The strength of the induced topotaxis depends on the occupied fraction λ , as the variation range of the diffusion constant upon changing α in Figs. 2(a) and 2(b) depends on the choice of λ . Consequently, an effective topotaxis based on the sliding angle can only be effective at large densities. While the idea of repeating blocks leads to a net flux for sliding-angle-based topotaxis, it results in localization near the borders for other topotaxis types (based on obstacle density, size, etc.) due to reflection at the borders of blocks.

We note that the values of α_1 and α_2 and the trajectories in Fig. 5 have been selected to highlight the effective reflection at the interface. Nevertheless, transport occurs in both directions in general, although with asymmetric probabilities $f_{1\rightarrow 2}$ and $f_{2\rightarrow 1}$ which depend on the geometrical parameters $\Delta\alpha$, α_{\min} , and λ but are independent of p . The Markov process of transport between these two zones eventually leads to steady-state probabilities $\rho_1 = f_{2\rightarrow 1}/(f_{1\rightarrow 2} + f_{2\rightarrow 1})$ and $\rho_2 = f_{1\rightarrow 2}/(f_{1\rightarrow 2} + f_{2\rightarrow 1})$ for residence in each zone. Although the explicit dependence of transition probabilities on topological properties of the medium is not known, their asymmetry is reflected in their ratio in the steady state, which is given as $\frac{f_{1\rightarrow 2}}{f_{2\rightarrow 1}} = \frac{\rho_2}{\rho_1}$. A strong topotaxis is gained for the set of conditions $\{\lambda \rightarrow 1, \Delta\alpha \gg 0, \text{ and } \alpha_{\min} \rightarrow 0\}$. Inversely, in sparse pillar parks or in the limit of $\Delta\alpha \rightarrow 0$, we obtain $\rho_1 \approx \rho_2 \approx \rho_s$ corresponding to a very weak topotaxis. As a final note, while the persistence affects neither the transition

probabilities nor the steady densities, it determines the time scale to reach the steady state; a particle with a larger p visits the interface more frequently, as it has a larger D .

IV. CONCLUSION

In summary, we have proposed a method to induce topotaxis over arbitrarily long distances by imposing a gradient of the sliding angle around obstacles. Such a gradient can be realized through coating for agents which form close contact with pillar surfaces (such as migrating cells). Cell-surface adhesion and cell migration dynamics at microscale are tunable, e.g., by changing the percentage of PLL-PEG coating [37]. Other topographic features can also be exploited depending on the nature of the agent-pillar interaction. For example, changing the slip condition at the pillar surface can affect the hydrodynamic interaction of swimming bacteria with pillars and, thus, the sliding distance over the pillar surface. Furthermore, the persistence dependence of the relaxation time to the steady state can be exploited to separate a mixture of microorganisms with different persistence. Our results are of technological and medical importance as a non-invasive method to design efficient taxis devices for guiding biological agents across vast distances.

ACKNOWLEDGMENT

This work was performed within and financially supported by the Collaborative Research Center SFB 1027 funded by the German Research Foundation.

-
- [1] J. Park, D.-H. Kim, and A. Levchenko, Topotaxis: A new mechanism of directed cell migration in topographic ECM gradients, *Biophys. J.* **114**, 1257 (2018).
- [2] J. A. J. Wondergem, M. Mytiliniou, F. C. H. de Wit, T. G. A. Reuvers, D. Holcman, and D. Heinrich, Chemotaxis and topotaxis add vectorially for amoeboid cell migration, *bioRxiv* 735779 (2021).
- [3] A. Reversat, F. Gaertner, J. Merrin, J. Stopp, S. Tasciyan, J. Aguilera, I. de Vries, R. Hauschild, M. Hons, M. Piel *et al.*, Cellular locomotion using environmental topography, *Nature (London)* **582**, 582 (2020).
- [4] M. Gorelashvili, M. Emmert, K. F. Hodeck, and D. Heinrich, Amoeboid migration mode adaption in quasi-3D spatial density gradients of varying lattice geometry, *New J. Phys.* **16**, 075012 (2014).
- [5] K. Schakenraad, L. Ravazzano, N. Sarkar, J. A. J. Wondergem, R. M. H. Merks, and L. Giomi, Topotaxis of active Brownian particles, *Phys. Rev. E* **101**, 032602 (2020).
- [6] M. T. Frey, I. Y. Tsai, T. P. Russell, S. K. Hanks, and Y. li Wang, Cellular responses to substrate topography: Role of myosin II and focal adhesion kinase, *Biophys. J.* **90**, 3774 (2006).
- [7] J.-P. Kaiser, A. Reinmann, and A. Bruinink, The effect of topographic characteristics on cell migration velocity, *Biomaterials* **27**, 5230 (2006).
- [8] M. J. Muthinja, J. Ripp, J. K. Hellmann, T. Haraszti, N. Dahan, L. Lemgruber, A. Battista, L. Schütz, O. T. Fackler, U. S. Schwarz *et al.*, Microstructured blood vessel surrogates reveal structural tropism of motile malaria parasites, *Adv. Healthc. Mater.* **6**, 1601178 (2017).
- [9] M. Chabaud, M. L. Heuzé, M. Bretou, P. Vargas, P. Maiuri, P. Solanes, M. Maurin, E. Terriac, M. Le Berre, D. Lankar *et al.*, Cell migration and antigen capture are antagonistic processes coupled by myosin II in dendritic cells, *Nat. Commun.* **6**, 7526 (2015).
- [10] M. R. Shaebani, R. Jose, L. Santen, L. Stankevics, and F. Lautenschläger, Persistence-speed coupling enhances the search efficiency of migrating immune cells, *Phys. Rev. Lett.* **125**, 268102 (2020).
- [11] P. Maiuri, J.-F. Rupprecht, S. Wieser, V. Rupprecht, O. Bénichou, N. Carpi, M. Coppey, S. De Beco, N. Gov, C.-P. Heisenberg *et al.*, Actin flows mediate a universal coupling between cell speed and cell persistence, *Cell* **161**, 374 (2015).
- [12] M. R. Shaebani, L. Stankevics, D. Vesperini, M. Urbanska, D. A. D. Flormann, E. Terriac, A. K. B. Gad, F. Cheng, J. E. Eriksson, and F. Lautenschläger, Effects of vimentin on the migration, search efficiency, and mechanical resilience of dendritic cells, *Biophys. J.* **121**, 3950 (2022).
- [13] L. Stankevics, N. Ecker, E. Terriac, P. Maiuri, R. Schoppmeyer, P. Vargas, A.-M. Lennon-Duménil, M. Piel, B. Qu, M. Hoth *et al.*, Deterministic actin waves as generators of cell polarization cues, *Proc. Natl. Acad. Sci. USA* **117**, 826 (2020).
- [14] M. R. Shaebani, M. Piel, and F. Lautenschläger, Distinct speed and direction memories of migrating dendritic

- cells diversify their search strategies, *Biophys. J.* **121**, 4099 (2022).
- [15] S. E. Spagnolie, G. R. Moreno-Flores, D. Bartolo, and E. Lauga, Geometric capture and escape of a microswimmer colliding with an obstacle, *Soft Matter* **11**, 3396 (2015).
- [16] T. Jakuszeit, O. A. Croze, and S. Bell, Diffusion of active particles in a complex environment: Role of surface scattering, *Phys. Rev. E* **99**, 012610 (2019).
- [17] O. Sipos, K. Nagy, R. Di Leonardo, and P. Galajda, Hydrodynamic trapping of swimming bacteria by convex walls, *Phys. Rev. Lett.* **114**, 258104 (2015).
- [18] Z. Sadjadi, D. Vesperini, A. M. Laurent, L. Barnefske, E. Terriac, F. Lautenschläger, and H. Rieger, Amoeboid cell migration through regular arrays of micropillars under confinement, *Biophys. J.* **121**, 4615 (2022).
- [19] D. Arcizet, S. Capito, M. Gorelashvili, C. Leonhardt, M. Vollmer, S. Youssef, S. Rappl, and D. Heinrich, Contact-controlled amoeboid motility induces dynamic cell trapping in 3D-microstructured surfaces, *Soft Matter* **8**, 1473 (2012).
- [20] X. Zhou, R. Zhao, K. Schwarz, M. Mangeat, E. C. Schwarz, M. Hamed, I. Bogeski, V. Helms, H. Rieger, and B. Qu, Bystander cells enhance NK cytotoxic efficiency by reducing search time, *Sci. Rep.* **7**, 44357 (2017).
- [21] V. Kantsler, J. Dunkel, M. Polin, and R. E. Goldstein, Ciliary contact interactions dominate surface scattering of swimming eukaryotes, *Proc. Natl. Acad. Sci. USA* **110**, 1187 (2013).
- [22] E. Lushi, V. Kantsler, and R. E. Goldstein, Scattering of biflagellate microswimmers from surfaces, *Phys. Rev. E* **96**, 023102 (2017).
- [23] M. Contino, E. Lushi, I. Tuval, V. Kantsler, and M. Polin, Microalgae scatter off solid surfaces by hydrodynamic and contact forces, *Phys. Rev. Lett.* **115**, 258102 (2015).
- [24] M. J. Saxton, Lateral diffusion in an archipelago: The effect of mobile obstacles, *Biophys. J.* **52**, 989 (1987).
- [25] M. J. Saxton, Anomalous diffusion due to obstacles: A Monte Carlo study, *Biophys. J.* **66**, 394 (1994).
- [26] J. Machta and R. Zwanzig, Diffusion in a periodic Lorentz gas, *Phys. Rev. Lett.* **50**, 1959 (1983).
- [27] Z. Sadjadi, M. Miri, M. R. Shaebani, and S. Nakhaee, Diffusive transport of light in a two-dimensional disordered packing of disks: Analytical approach to transport mean free path, *Phys. Rev. E* **78**, 031121 (2008).
- [28] P. Tierno and M. R. Shaebani, Enhanced diffusion and anomalous transport of magnetic colloids driven above a two-state flashing potential, *Soft Matter* **12**, 3398 (2016).
- [29] L. Dagdug, M.-V. Vazquez, A. M. Berezhkovskii, V. Yu. Zitserman, and S. M. Bezrukov, Diffusion in the presence of cylindrical obstacles arranged in a square lattice analyzed with generalized Fick-Jacobs equation, *J. Chem. Phys.* **136**, 204106 (2012).
- [30] M. R. Shaebani, H. Rieger, and Z. Sadjadi, Kinematics of persistent random walkers with two distinct modes of motion, *Phys. Rev. E* **106**, 034105 (2022).
- [31] A. E. Hafner, L. Santen, H. Rieger, and M. R. Shaebani, Run-and-pause dynamics of cytoskeletal motor proteins, *Sci. Rep.* **6**, 37162 (2016).
- [32] M. R. Shaebani and H. Rieger, Transient anomalous diffusion in run-and-tumble dynamics, *Front. Phys.* **7**, 120 (2019).
- [33] Z. Sadjadi and M. R. Shaebani, Orientational memory of active particles in multistate non-Markovian processes, *Phys. Rev. E* **104**, 054613 (2021).
- [34] M. R. Shaebani, Z. Sadjadi, I. M. Sokolov, H. Rieger, and L. Santen, Anomalous diffusion of self-propelled particles in directed random environments, *Phys. Rev. E* **90**, 030701(R) (2014).
- [35] A. Wysocki, A. K. Dasanna, and H. Rieger, Interacting particles in an activity landscape, *New J. Phys.* **24**, 093013 (2022).
- [36] M. J. Schnitzer, Theory of continuum random walks and application to chemotaxis, *Phys. Rev. E* **48**, 2553 (1993).
- [37] Y.-J. Liu, M. Le Berre, F. Lautenschläger, P. Maiuri, A. Callan-Jones, M. Heuzé, T. Takaki, R. Voituriez, and M. Piel, Confinement and low adhesion induce fast amoeboid migration of slow mesenchymal cells, *Cell* **160**, 659 (2015).